Defense Technical Information Center Compilation Part Notice

ADP011202

TITLE: Low-Temperature Electrodep-osition of the High-Temperature Cubic Polymorph of Bismuth[III] Oxide

DISTRIBUTION: Approved for public release, distribution unlimited

This paper is part of the following report:

TITLE: Internal Workshop on Interfacially Controlled Functional Materials: Electrical and Chemical Properties Held in Schloss Ringberg, Germany on March 8-13, 1998

To order the complete compilation report, use: ADA397655

The following component part numbers comprise the compilation report:
ADP011194 thru ADP011211

ELSEVIER

Solid State Ionics 131 (2000) 97–107

SOLID STATE IONICS

www.elsevier.com/locate/ssi

Low-temperature electrodeposition of the high-temperature cubic polymorph of bismuth(III) oxide

Eric W. Bohannan, Christopher C. Jaynes, Mark G. Shumsky, Julie K. Barton, Jay A. Switzer*

University of Missouri-Rolla, Department of Chemistry and Graduate Center for Materials Research, Rolla, MO 65409-1170, USA

Received 1 September 1999; received in revised form 1 November 1999; accepted 1 December 1999

Abstract

Nanocrystalline films of δ-Bi_2O_3 were electrodeposited at 65°C directly from alkaline solutions of tartrate-complexed Bi(III). This face-centered-cubic polymorph of Bi_2O_3 is normally only stable at high temperatures (729–825°C). The material has the highest known oxide ion mobility. We propose that the high temperature form of the oxide is stabilized due to the nanocrystalline (70 nm) size of the particles in the film. The oxide also deposits epitaxially onto a single-crystal Au(110) substrate with strong in-plane and out-of-plane orientation. The large lattice mismatch (35.4%) is accommodated by forming a coincidence lattice, in which the δ-Bi_2O_3 is rotated 90° relative to the Au (110) substrate. The epitaxial relationship between film and substrate may also serve to stabilize the high-temperature structure.

Keywords: Bismuth oxide; Electrodeposition; Epitaxial growth; Solid electrolyte

PACS: 81.15.P (Electrodeposition)

1. Introduction

Oxide-ion conducting solid electrolytes are of great interest for use in fuel cells, oxygen sensors, and oxygen pumps. The most widely used solid electrolytes with high oxide ion conductivity are those derived from zirconia, with yttria-stabilized zirconia being the most widely applied. However, zirconia-based solid electrolytes have an oxide ion conductivity that is up to two orders of magnitude lower than the cubic form of Bi_2O_3 [1]. A significant limitation of the bismuth oxide system is that the face-centered-cubic phase exists only between 729°C and the melting point of the material, 825°C [2]. Substitution of rare-earth oxides stabilizes δ-Bi_2O_3 down to room temperature, however there is a coincident lowering of the oxide ion conductivity by over two orders of magnitude [3].

The polymorphism of pure bismuth sesquioxide has been studied by several investigators [4–8] since the work of Sillén [9], who proposed that four polymorphs exist. Below 729°C Bi_2O_3 exists as the monoclinic α-phase. When cooling from temperatures above 729°C, the face-centered cubic (fcc)

*Corresponding author. Tel.: +1-573-341-4383; fax: +1-573-341-4383.

E-mail address: jswitzer@umr.edu (J.A. Switzer)

0167-2738/00/$ – see front matter
PII: S0167-2738(00)00625-1

δ-phase of Bi_2O_3 has been observed to undergo a transformation into one of two metastable phases, the tetragonal β-phase or the body centered cubic (bcc) γ-phase, before reverting to the monoclinic form. Sillen first described δ-Bi_2O_3 as having a pseudo-fluorite structure with one quarter of the oxygen atoms missing in an ordered defect oxygen lattice [9]. Gattow and Schröder showed by X-ray powder diffraction that δ-Bi_2O_3 is fcc and rejected the ordered defects in the oxygen lattice, preferring instead a statistical occupancy of 75% on each anion site [10]. Willis proposed a more complicated model in which each anion site is replaced by four equivalent sites displaced from their ideal positions, each site having an occupancy factor of 3/16 [11]. Battle et al. have shown by refinement of neutron diffraction patterns that δ-Bi_2O_3 has a highly defective fluorite structure where 43% of the regular anion sites are occupied, in addition to 8% occupancy of a second site displaced from the regular anion position [12]. The unusually high ionic conductivity of δ-Bi_2O_3 has been attributed to the highly disordered oxygen sublattice [13].

Electrodeposition as a means of materials synthesis offers the advantages of low processing temperatures, control of film thickness, deposition onto complex shapes, low capital investment and the production of nonequilibrium materials that cannot be accessed by traditional thermal processing. We have previously used electrodeposition to create superlattices of metal oxides [14–16] and nonequilibrium layered nanostructures of Cu_2O and Cu which showed quantum confinement effects in electrical properties [17–21]. Recently, we reported that epitaxial films of δ-Bi_2O_3 can be electrodeposited on Au single crystal substrates at 65°C, with the material stabilized by a template effect [22]. The production of room temperature stable epitaxial δ-Bi_2O_3 nanoscopic mesas grown by pulsed laser deposition has also been reported [23]. Nonequilibrium materials can be stabilized by the production of nanometer-scale crystallites, as in the case of ZrO_2 [24–27], or by epitaxially electrodepositing the material onto a substrate with a crystal structure similar to that of the desired product. In this work, we produce δ-Bi_2O_3 by electrodeposition that is stabilized at room temperature due to the nanoscale crystallites that are formed. We also show that the structure can be epitaxially stabilized by electrodepositing δ-Bi_2O_3 onto single crystal Au. The epitaxial films are shown to be oriented in-plane and out-of-plane by X-ray diffraction techniques.

2. Experimental procedure

Each 500-ml deposition solution consisted of 0.1 M Bi(III) nitrate pentahydrate, 0.25 M tartaric acid, and 2.5 M KOH prepared with water (>18 MΩ) from a Barnstead NANOpure ultra pure water system. All chemicals were reagent grade and purchased from Aldrich. Temperature control was maintained with a Cole Palmer model 04644 digital hot plate/stirrer with temperature probe. A constant temperature of 65°C in the stirred solution was maintained during electrodeposition.

Electrodeposition was performed with an EG and G Princeton Applied Research Model 273A potentiostat/galvanostat. A three-electrode electrochemical cell was employed consisting of a working electrode (430 stainless steel, polycrystalline Au or single crystal Au), a saturated Ag/AgCl reference electrode and a Pt-wire counter electrode. The electropolished Au single crystal was purchased from Monocrystals Company. The single crystal had a 10-mm diameter and a 1-mm thickness. The purity of the Au was 99.99 + %. Commercially available 9-MHz AT-cut quartz crystals (Seiko EG and G model QA-AM9-AU) were used as the working electrode during electrochemical quartz crystal microbalance (EQCM) experiments. The quartz crystals have a coating on both sides consisting of a 500 Å Ti layer beneath a 3000 Å layer of Au. The quartz crystals were installed in a Teflon holder so that only one electrode face, with an area of 0.20 cm^2 was exposed to the solution. A quartz crystal analyzer (Seiko EG and G model QCA917) was used in conjunction with a Nicolet Pro10 oscilloscope to monitor changes in frequency during experiments. A gate time of 0.1 s and an output range of ±20 KHz/10 V was used with the analyzer. For all depositions a constant anodic current density of 5 mA/cm^2 was applied.

X-ray diffraction (XRD) experiments were performed with a Scintag 2000 diffractometer using CuKα radiation. Rietveld refinement of the powder

diffraction pattern of δ-Bi_2O_3, obtained from a series of films grown on 430 stainless steel, was performed with commercially available RIQAS software. Azimuthal scans of epitaxial films were obtained by the use of a texture goniometer accessory that had been fashioned in-house for the Scintag 2000. Particle size and strain measurements were obtained using the program SHADOW (Ver. 4.00, Materials Data). Instrumental broadening was determined with a LaB_6 standard (SRM 660) purchased from NIST.

A Hitachi S-570 scanning electron microscope (SEM) was used to obtain cross-sectional images of the δ-Bi_2O_3 films. The SEM was operated with an accelerating voltage of 25 kV and a magnification of 40 000×. Prior to imaging, the samples were sputter coated with ~100 Å of 60% Au/40% Pd to prevent sample charging. Energy dispersive spectroscopy (EDS) measurements were performed on uncoated samples with an EDAX Phoenix system in conjunction with a Hitachi S-4700 field emission SEM. Atomic force microscopy (AFM) images were obtained with a Digital Nanoscope E scanning probe microscope which was operated in the contact mode. The samples were imaged in air with Au-coated Si_3N_4 probes.

3. Results and discussion

The XRD powder pattern for electrodeposited δ-Bi_2O_3 is shown in Fig. 1. The powder sample was obtained from numerous thin films removed from 430 stainless steel substrates. A Rietveld fit to the powder pattern was performed with RIQAS software and is also shown. The Rietveld fit was performed with space group Fm3m, with the Bi atoms at (0,0,0), and oxygen atoms at (0.25,0.25,0.25) and (0.354,0.354,0.354) with occupancies of the oxygen sites of 0.43 and 0.08, respectively. Refinement of the pattern gave residual errors of 7.62% and 11.10% for R and R_{wp}. It is of note that a similar refinement performed with the same parameters except with the oxygens only at (0.25,0.25,0.25) and an occupancy of 0.75 gave similar residual errors ($R = 7.93\%$, $R_{wp} = 11.72\%$). The scattering factor for oxygen is much less than that of Bi, so very little can be learned about the precise placement of the oxygen atoms by XRD. A precision lattice parameter of 5.531±0.001 Å was determined by high angle X-ray diffraction using a silicon reference standard. The lattice parameter for thermally prepared δ-Bi_2O_3 at 1047 K is 5.6595 Å [3]. Taking into account the

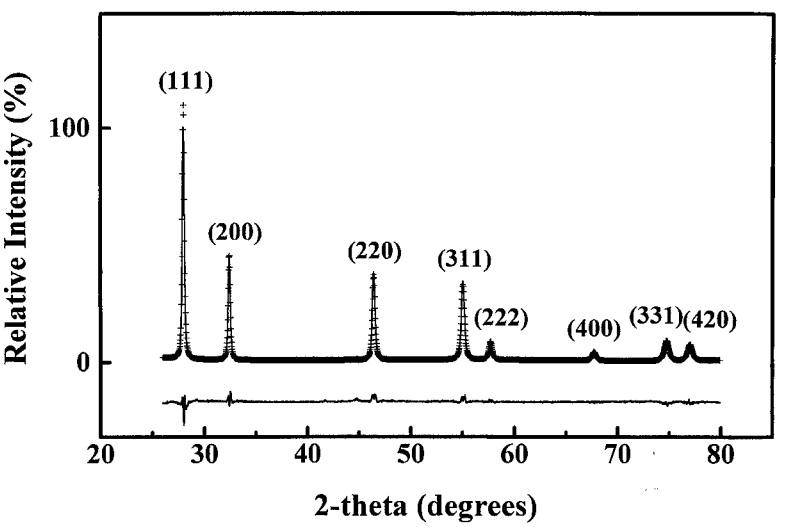

Fig. 1. XRD powder pattern (solid line), Rietveld fit (+), and difference pattern for δ-Bi_2O_3. A space group of *Fm3m* was assigned, with bismuth atoms at (0,0,0) and oxygen atoms on two sites, (0.25,0.25,0.25) and (0.354,0.354,0.354) with occupancies of 0.43 and 0.08, respectively.

thermal expansion coefficient for δ-Bi_2O_3 of 2.4×10^{-5} K^{-1} [5], the lattice parameter of our electrodeposited δ-Bi_2O_3 extrapolated to 1047 K is 5.6 Å. We view this as good agreement between the two materials, given the uncertainty in the expansion coefficient and the large degree of extrapolation required. The room-temperature positions and intensities of the observed reflections for electrodeposited δ-Bi_2O_3 powder are given in Table 1.

The cubic form of δ-Bi_2O_3 may be stabilized at these low temperatures by the small particle size of crystallites in the film. X-ray line broadening can be used to determine strain and particle size of a given crystalline material. Using the method developed by Williamson and Hall [28], the contributions of the particle size and strain to the observed X-ray line broadening, β, are considered to be additive.

$$\beta_{\text{total}} = \beta_{\text{particle size}} + \beta_{\text{strain}} \quad (1)$$

The contribution of broadening due to small particle size is given by the Scherrer equation while the broadening due to strain is represented by differentiation of the Bragg law.

$$\beta_{\text{total}} = \frac{0.94\lambda}{t \cos\theta} + 4 \tan\theta(\Delta d/d) \quad (2)$$

Table 1
Powder X-ray diffraction of electrodeposited δ-Bi_2O_3[a]

(*hkl*)	*d*-Spacing (Å)	2-Theta (degrees)	Relative intensity (%)
(111)	3.193	27.94	100
(200)	2.766	32.37	46
(220)	1.956	46.43	47
(311)	1.668	55.07	50
(222)	1.597	57.74	12
(400)	1.383	67.77	6
(331)	1.269	74.82	16
(420)	1.237	77.12	13
(422)	1.129	86.13	10
(511) (333)	1.064	92.81	13

[a] Positions calculated using crystallographically determined precision lattice parameter ($a = 5.531$ Å) and measured relative intensities observed in the room-temperature powder X-ray diffraction pattern for electrodeposited δ-Bi_2O_3 using a CuKα ($\lambda = 1.5418$ Å) source.

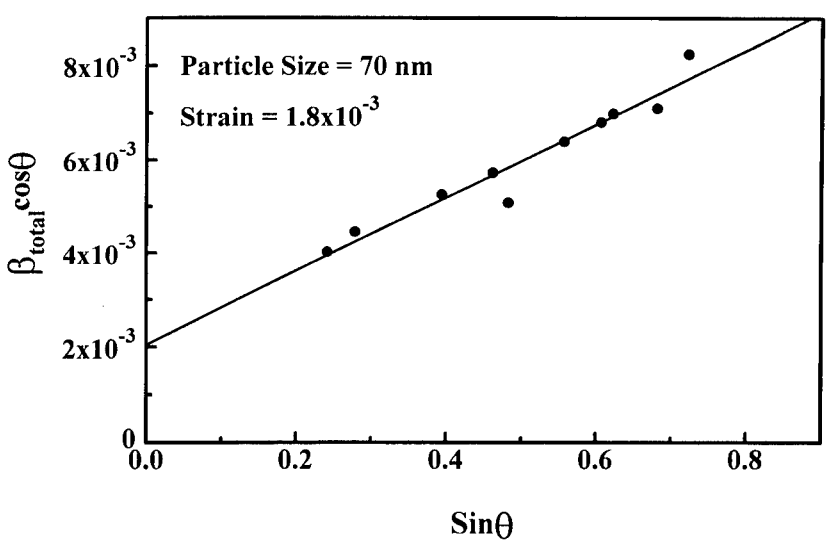

Fig. 2. Williamson–Hall plot for δ-Bi_2O_3 from X-ray powder pattern. A particle size of 70 nm was obtained from the *y*-intercept of the plot, while the strain ($\Delta d/d$) was determined from the slope of the line to be 1.8×10^{-3}. Linear regression gave a correlation coefficient of 0.97.

The total broadening (β_{total}) is the measured fwhm in radians, corrected for instrumental broadening. The X-ray wavelength of the source (CuKα=0.154 nm) is given by λ, t is the particle size, and $\Delta d/d$ represents the strain. Multiplying both sides of Eq. (2) by cos θ gives the final form,

$$\beta_{total}\cos\theta = \frac{0.94\lambda}{t} + 4\sin\theta(\Delta d/d) \quad (3)$$

which is used to calculate the particle size and strain for δ-Bi_2O_3 from a plot of β_{total} cos θ versus sin θ, as shown in Fig. 2. Using the y-intercept obtained from linear regression of the broadening as a function of diffraction angle, we obtained a particle size of 70 nm. The slope of the fitted line gives a strain of 1.8×10^{-3} in the powder. The nanocrystalline nature of these films, as well as the strain observed, may help explain the stabilization of the fcc structure for Bi_2O_3 at room temperature.

We have also used the electrochemical chemical quartz crystal microbalance (EQCM) as an in situ monitor of δ-Bi_2O_3 film growth. The EQCM allows for the determination of minute mass changes, down to the sub-nanogram range, by monitoring the frequency response of a quartz oscillator during the electrodeposition process. The piezoelectric device, coated with Au, was used as the working electrode during the electrodeposition of δ-Bi_2O_3. The Sauerbrey equation [Eq. (4)] describes the mass-frequency relationship for the EQCM.

$$\Delta f = \frac{-2f_o^2\,\Delta m}{(\rho\mu)^{1/2}A} \quad (4)$$

The measured frequency shift is given by Δf, f_o is the resonant frequency of the oscillator (9 MHz), Δm is the mass change, ρ is the density of quartz (2.648 g/cm^3), μ is the shear modulus of quartz (2.947×10^{11} dyn/cm^2), and A is the piezoelectrically active area.

Fig. 3 shows the potential transient, the mass accumulated at the electrode, and the calculated thickness of a δ-Bi_2O_3 film during electrodeposition at a constant anodic current density of 5 mA/cm^2. The crystallographic density of δ-Bi_2O_3 (9.17 g/cm^3), was used in conjunction with the mass deposited to calculate the thickness of the film, assuming the film to be 100% dense. After an initial induction period, the potential increases sharply as mass begins accumulating on the electrode. As the deposition proceeds there is a gradual decrease in the rate of deposition, as evidenced by the decrease in slope in parts B and C of Fig. 3. This is most likely due to a competing reaction of oxygen evolution at the working electrode.

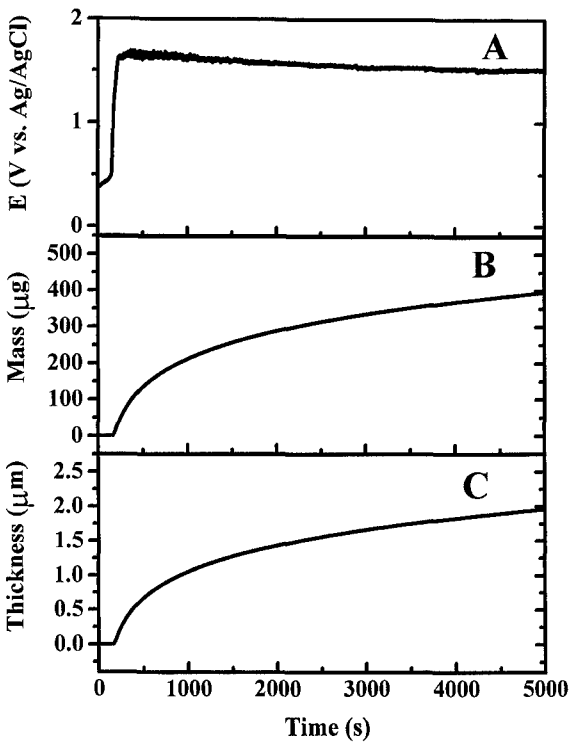

Fig. 3. In-situ monitoring of δ-Bi_2O_3 electrodeposition. Part A shows the potential transient vs. a Ag/AgCl reference electrode at a constant anodic current density of 5 mA/cm^2. Part B shows the mass accumulated at the electrode surface as a function of deposition time as determined with the EQCM. Part C shows the thickness of the electrodeposited δ-Bi_2O_3 film as calculated from the EQCM data and the crystallographic density of δ-Bi_2O_3 (9.17 g/cm^3).

At this point, the mechanism of δ-Bi_2O_3 deposition has not been clearly elucidated. Pourbaix has suggested that under strongly alkaline conditions the Bi(III) species existing in solution is BiO_2^- and that Bi(III) can be oxidized to Bi(V) through electrolytic means [29]. We propose the following possible mechanism.

$$2BiO_2^- + 2OH^- \rightarrow Bi_2O_5 + H_2O + 4e^- \quad (5)$$

$$Bi_2O_5 \rightarrow \delta\text{-}Bi_2O_3 + O_2 \quad (6)$$

In Eq. (5) we show the oxidation of the solution species to bismuth(V) oxide. This film then undergoes an internal redox reaction, decomposing to form δ-Bi_2O_3 while evolving oxygen gas. In agreement with this mechanism, if the deposition is carried out at temperatures between 50°C and room temperature, reddish-brown amorphous films are obtained on the electrode surface. The color is consistent with that of bismuth(V) oxide [30] and the films also give a positive iodometric response. Assuming this mechanism, the instantaneous current efficiency of the deposition process was calculated as a function of thickness as shown in Fig. 4. From a maximum current efficiency of approximately 55% during the early stages of deposition, the current efficiency falls off to a value of approximately 2% at 5000 s. This falloff may be due to a competing reaction, the evolution of oxygen at the working electrode, which is shown in Eq. (7).

$$4OH^- \rightarrow O_2 + 2H_2O + 4e^- \quad (7)$$

Vigorous gas evolution was observed at the working electrode surface during the later stage of film deposition, consistent with Eq. (7). The nominal thickness of this film, grown for 5000 s, is 2 μm. Because the current efficiency decreases with deposition time, it is not possible under the present conditions to grow films with a thickness much larger than 2 μm.

The XRD pattern for the film used in the EQCM experiments is shown in Fig. 5. The substrate is a gold-coated EQCM electrode, used as received from the manufacturer. The gold film shows a strong (111) preferred orientation. Fig. 5 clearly shows that the δ-Bi_2O_3 also has a strong (111) orientation suggestive of an epitaxial relationship between Au and the electrodeposited film. A SEM micrograph of a cross-section of the δ-Bi_2O_3 film is shown in Fig. 6. The cross-section reveals a columnar microstructure, consistent with a highly oriented thin film. Several cross-sectional images, obtained from different regions of the film, revealed that the film has good thickness uniformity. The film thickness, determined from the SEM micrograph, is approximately 2 μm. This is in good agreement with the value calculated from the EQCM data. In order to determine the crystallite sizes present in the film, an image of the surface of the film was obtained with an AFM operated in the contact mode as shown in Fig.

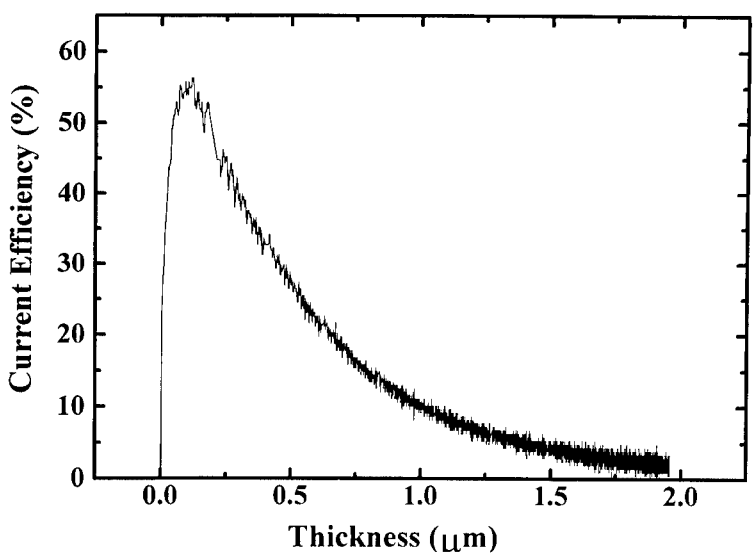

Fig. 4. Current efficiency of the δ-Bi_2O_3 electrodeposition process as a function of film thickness. The current efficiency was determined using EQCM data, the applied current density, and the proposed mechanism given in the text. The fall off in current efficiency reveals that the films can be grown only to a nominal thickness of 2 μm.

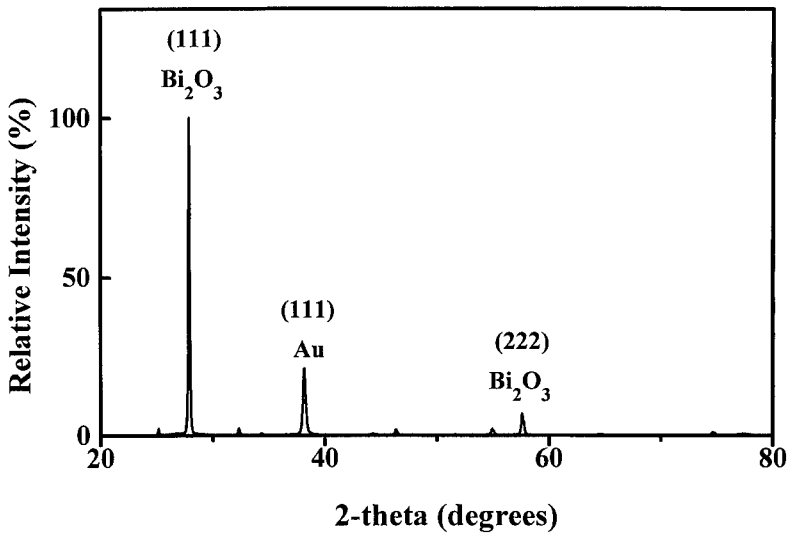

Fig. 5. XRD pattern of a δ-Bi_2O_3 deposited onto a (111)-textured Au EQCM electrode. Comparison of this pattern with that shown in Fig. 1 reveals that the δ-Bi_2O_3 has a strong (111) preferred orientation, suggestive of an epitaxial relationship between Au and δ-Bi_2O_3.

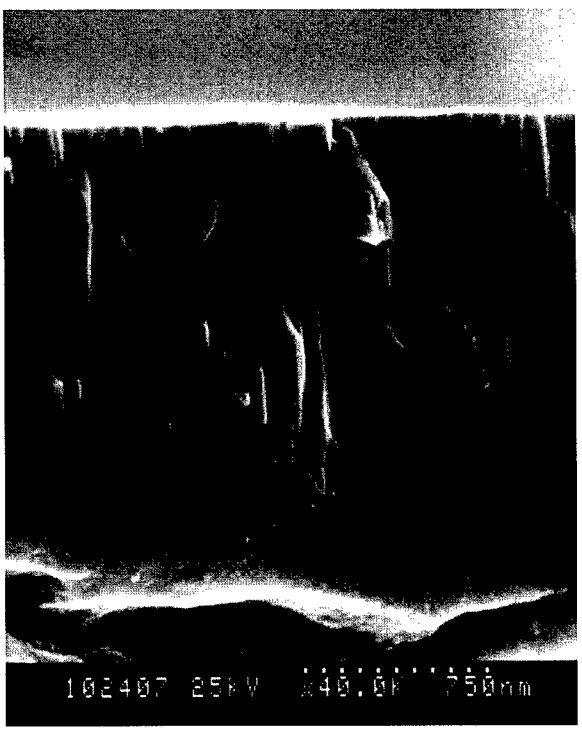

Fig. 6. SEM cross-sectional image of δ-Bi_2O_3 electrodeposited onto a (111)-textured Au EQCM electrode. The image shows a high degree of columnar growth, typical of textured films. The thickness of the film as determined by SEM agrees well with that calculated from the EQCM. The bar marker is 750 nm.

7. The average crystallite size was 65±6 nm, which is in agreement with the particle size obtained from Williamson–Hall analysis of the δ-Bi_2O_3 powder sample discussed earlier. EDS showed no evidence of K incorporation in the δ-Bi_2O_3 film, consistent with the structure being stabilized due to small crystallite size and not to the presence of dopants. Standardless quantification of the O/Bi ratio by EDS gave a stoichiometry of $Bi_2O_{2.9}$.

Although there is the hint of an epitaxial relationship between Au and δ-Bi_2O_3 seen in Fig. 5, in order to confirm this relationship it is necessary to show that the two materials have both in-plane and out-of-plane alignment. This was accomplished by electrodepositing δ-Bi_2O_3 onto a Au(110) single crystal substrate. The θ–2θ pattern for a δ-Bi_2O_3 film grown on a Au(110) single crystal is shown in Fig. 8. For the Au substrate, only the (220) reflection is observed over the diffraction angles shown. The δ-Bi_2O_3 shows mainly the (220) and (440) reflections, indicating that there is a strong out-of-plane epitaxial relationship. It has been suggested that the high-temperature form of δ-Bi_2O_3 has a primitive cubic as opposed to a face centered cubic structure [31]. The observation of mixed index reflections would preclude a face centered cubic structure for our material, as these reflections are symmetry

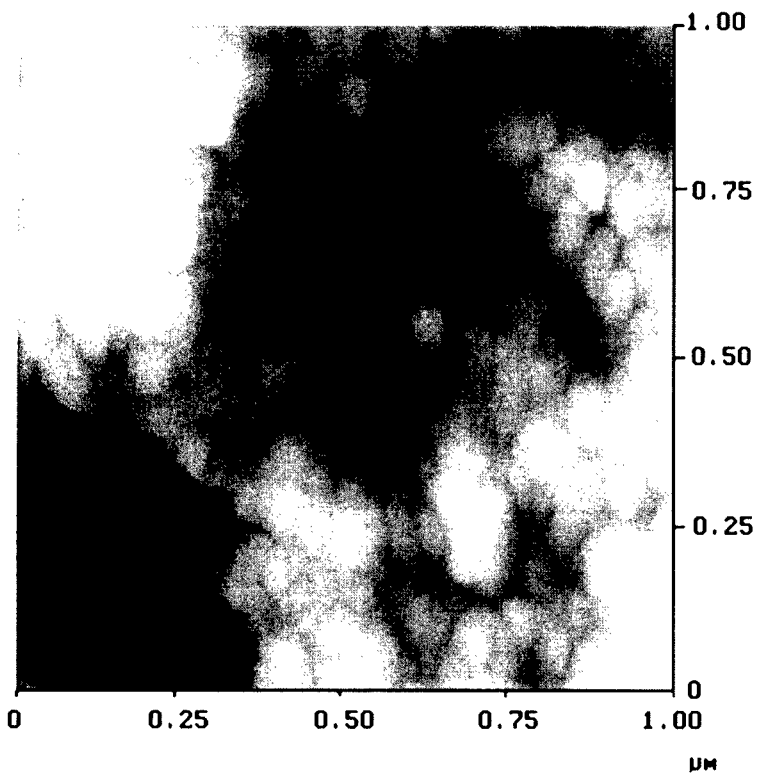

Fig. 7. Contact AFM image of the surface of an electrodeposited δ-Bi_2O_3 film grown on a (111) textured Au EQCM electrode. The scan size is 1.0 μm in both directions. The average particle size is 65±6 nm.

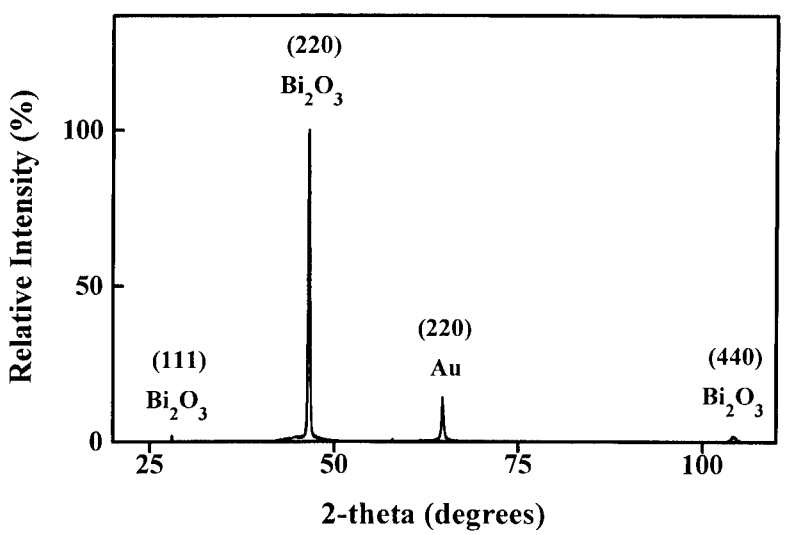

Fig. 8. XRD pattern of a δ-Bi_2O_3 film electrodeposited onto a Au(110) single crystal. The δ-Bi_2O_3 shows a strong (110) out-of-plane orientation, following the orientation of the Au single crystal. The absence of the (110) reflection for Bi_2O_3 precludes the δ-Bi_2O_3 structure from being primitive cubic.

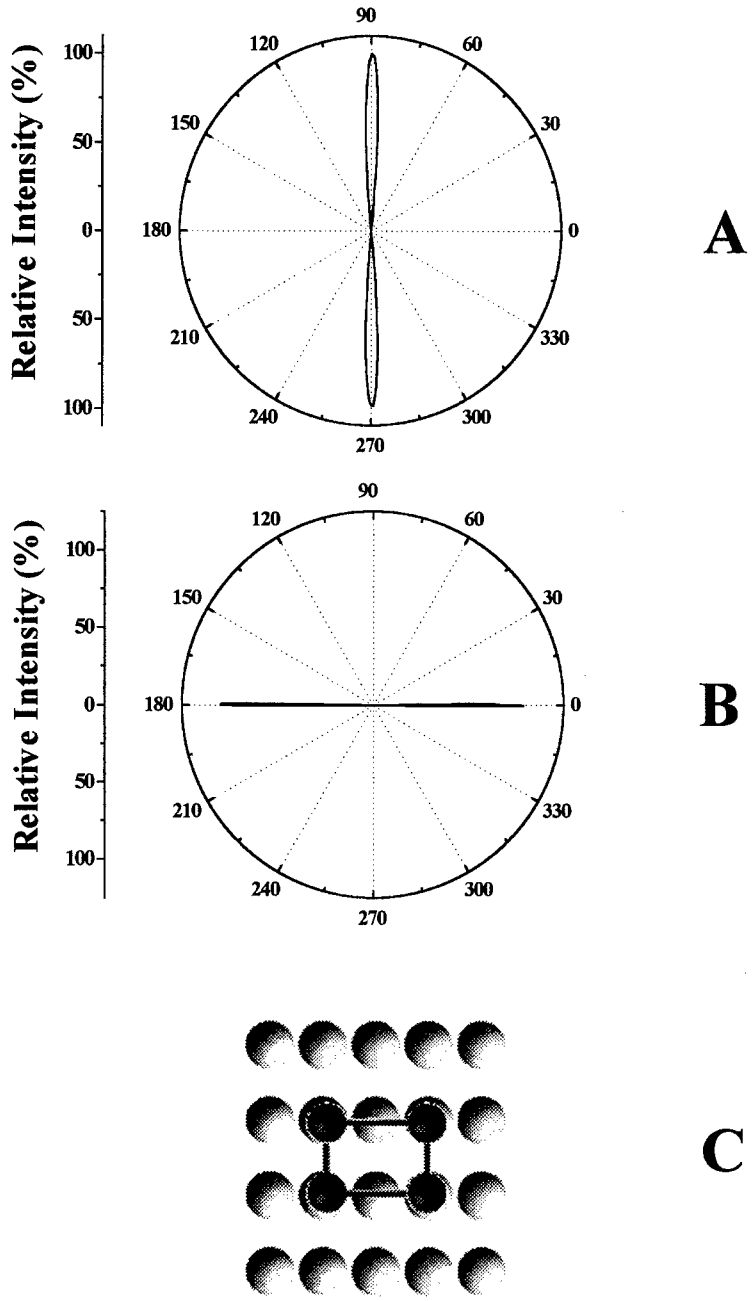

Fig. 9. Evidence for in-plane orientation in electrodeposited δ-Bi_2O_3. Part A shows the azimuthal scan for the (200) δ-Bi_2O_3 reflection for a film deposited onto single crystal Au(110). The azimuthal scan shows the expected two-fold symmetry and shows a high degree of in-plane orientation. Part B shows the azimuthal scan for the (200) reflection of the Au(110) single crystal substrate. Two-fold symmetry is again observed, although, comparing parts A and B, the peaks of δ-Bi_2O_3 are rotated 90° relative to the Au substrate. For both azimuthal scans, the sample was tilted at an angle of 45° to bring the (200) reflections into the Bragg condition. Part C shows an interface model for epitaxial growth of δ-Bi_2O_3 on Au. The δ-Bi_2O_3 overlayer (bismuth atoms represented as dark balls) is rotated 90° relative to the Au substrate. This $(1\times1)Bi_2O_3(110)[110]//(2\times1)Au(110)[100]$ coincidence lattice reduces the lattice mismatch from 35.4% to −4.2%.

forbidden. However, there is no evidence of a (110) reflection for epitaxial δ-Bi_2O_3 as the baseline noise at the expected spacing for the (110) reflection is less than 0.1% of the intensity seen for the (220) δ-Bi_2O_3 reflection. Therefore, our material is rigorously face-centered-cubic.

If there is a true epitaxial relationship between film and sample, the film grown on single crystal Au should also show evidence of in-plane orientation. The in-plane (parallel to the substrate) orientation of the δ-Bi_2O_3 film on (110) single crystal Au was examined by performing azimuthal (ϕ) X-ray scans. In order to bring other reflections, besides the (110) family, into the Bragg condition, it is necessary to tilt the sample at an appropriate angle. For the present sample, in order to observe the (100) family of reflections, it is necessary to tilt the sample at an angle of 45°, which corresponds to the angle between the [100] and [110] directions. By setting 2θ equal to 32.39°, which corresponds to the (200) reflection for δ-Bi_2O_3, and rotating the tilted sample, an azimuthal scan is obtained as shown in Fig. 9. The azimuthal scan is essentially a cross-section of the pole figure at a given tilt angle. Part A of Fig. 9 shows the azimuthal scan for the (200) reflection of δ-Bi_2O_3. The two-fold symmetry that is observed is proof of in-plane orientation and hence the epitaxial relationship between film and substrate. Part B shows the azimuthal scan for the (200) reflection of Au (2θ= 44.39°), which was also obtained at a tilt angle of 45°. As expected, two-fold symmetry is observed in the ϕ scan, however the film peaks of part A are rotated 90° relative to the substrate peaks of part B. This is explained by examining closely the lattice mismatch of the system. By only comparing the lattice parameters of Au and δ-Bi_2O_3, a lattice mismatch of 35.4% is calculated. This mismatch is so large that any epitaxial relationship between the two would be extremely unlikely. However, if we compare the spacing between Au atoms along the [100] direction (0.40786 nm), and the spacing of Bi atoms along the [110] direction (0.3907 nm), the lattice mismatch is much smaller (−4.2%). This situation requires rotation of the film 90° relative to the substrate, forming a $(1\times1)Bi_2O_3(110)[110]//(2\times1)Au(110)[100]$ coincidence lattice, a representation of which is shown in Fig. 9c. We have examined other samples grown on the other low-index faces of single crystal Au substrates, with these revealing much more complicated epitaxial relationships [22]. The epitaxial relationship between fcc Au and δ-Bi_2O_3 may stabilize the fcc phase at room temperature by a template effect.

4. Conclusions

We have shown that thin films of δ-Bi_2O_3 can be electrodeposited directly from an alkaline Bi(III) tartrate solution. Normally observed only between the temperatures of 729 and 825°C, the electrodeposited δ-Bi_2O_3 films in this study are stable at room temperature. This unexpected stability of the high temperature phase may be due to the nanocrystalline nature of the films. The films may also be epitaxially stabilized, as observed by the formation of a coincidence lattice of δ-Bi_2O_3 on single-crystal Au(110). These films should be of great interest, since δ-Bi_2O_3 has the highest oxide ion conductivity of any material studied to date.

Acknowledgements

This work was supported by Office of Naval Research grant N00014-96-1-0984, National Science Foundation grants CHE-9816484 and DMR-9704288, and the University of Missouri Research Board.

References

[1] T. Takahashi, H. Iwahara, Mat. Res. Bull. 13 (1978) 1447.
[2] H.A. Harwig, A.G. Gerards, Thermochim. Acta 28 (1979) 121.
[3] P. Shuk, H.D. Wiemhöfer, U. Guth, W. Göpel, M. Greenblatt, Solid State Ionics 89 (1996) 179.
[4] W.C. Schumb, E.S. Rittner, J. Am. Chem. Soc. 65 (1943) 1055.
[5] E.M. Levin, R.S. Roth, J. Res. Natl. Bur. Std. 68A (2) (1964) 189.
[6] E.M. Levin, R.S. Roth, J. Res. Natl. Bur. Std. 68A (2) (1964) 197.
[7] C.N.R. Rao, G.V. Subba Rao, S. Ramdas, J. Phys. Chem 73 (3) (1969).
[8] H.A. Harwig, Z. Anorg. Allg. Chem. 444 (1978) 151.
[9] L.G. Sillén, Ark. Kemi Mineral. Geol. 12A (18) (1937) 1.

[10] G. Gattow, H. Schröder, Z. Anorg. Allg. Chem. 318 (1962) 176.
[11] B.T.M. Willis, Acta Crystallogr. 18 (1965) 75.
[12] P.D. Battle, C.R.A. Catlow, J. Drennan, A.D. Murray, J. Phys. C 16 (1983) L561.
[13] L.A. Depero, L. Sangaletti, J. Solid State Chem. 122 (1996) 439.
[14] J.A. Switzer, M.J. Shane, R.J. Phillips, Science 247 (1990) 444.
[15] J.A. Switzer, R.P. Raffaelle, R.J. Phillips, C.-J. Hung, T.D. Golden, Science 258 (1992) 1918.
[16] J.A. Switzer, C.-J. Hung, B.E. Breyfogle, M.G. Shumsky, R. Van Leeuwen, T.D. Golden, Science 264 (1994) 1573.
[17] J.A. Switzer, C.-J. Hung, L.-Y. Huang, E.R. Switzer, D.R. Kammler, T.D. Golden, E.W. Bohannan, J. Am. Chem. Soc. 120 (1998) 3530.
[18] J.A. Switzer, B.M. Maune, E.R. Raub, E.W. Bohannan, J. Phys. Chem. B 103 (1999) 395.
[19] E.W. Bohannan, L.-Y. Huang, F.S. Miller, M.G. Shumsky, J.A. Switzer, Langmuir 15 (1999) 813.
[20] J.A. Switzer, C.-J. Hung, L.-Y. Huang, F.S. Miller, Y. Zhou, E.R. Raub et al., J. Mater. Res. 13 (1998) 909.
[21] J.A. Switzer, C.-J. Hung, E.W. Bohannan, M.G. Shumsky, T.D. Golden, D.C. Van Aken, Adv. Mater. 9 (1997) 334.
[22] J.A. Switzer, M.G. Shumsky, E.W. Bohannan, Science 284 (1999) 293.
[23] M. Alexe, J.F. Scott, C. Curran, N.D. Zakharov, D. Hesse, A. Pignolet, Appl. Phys. Lett. 73 (1998) 1592.
[24] R.C. Garvie, J. Phys. Chem. 69 (1965) 1238.
[25] K.S. Mazdiyasni, C.T. Lynch, J.S. Smith, J. Am. Ceram. Soc. 48 (1964) 372.
[26] T. Mitsuhashi, M. Ichihara, U. Tatsuke, J. Am. Ceram. Soc. 57 (1974) 97.
[27] J.A. Switzer, R.J. Phillips, Mat. Res. Soc. Symp. Proc. 121 (1988) 111.
[28] G.K. Williamson, W.H. Hall, Acta Metallurgica 1 (1953) 22.
[29] J. Van Muylder, M. Pourbaix, in: Atlas of Electrochemical Equilibria in Aqueous Solutions, Pergamon Press, New York, 1966, pp. 533–539.
[30] F.G. Cotton, G. Wilkinson, in: Advanced Inorganic Chemistry, 5th Edition, John Wiley and Sons, New York, 1988, pp. 401–402.
[31] J.W. Medernach, R.L. Snyder, J. Am. Ceram. Soc. 61 (1978) 494.